The role of Excess Sn in $Cu_4Sn_7S_{16}$ for the modification in band structures and reduction in lattice thermal conductivity

Tongtong He[a,b], Naiming Lin[a,*], Zhengliang Du[b], Yimin Chao[c,*], Jiaolin Cui[b,*]

[a] Materials Science and Engineering College, Taiyuan University of Technology, Taiyuan, 030024, China

[b] School of Materials & Chemical Engineering, Ningbo University of Technology, Ningbo, 315016, China

[c] School of Chemistry, University of East Anglia, Norwich NR4 7TJ, United Kingdom

ABSTRACT In this work we have investigated the band structures of ternary $Cu_4Sn_{7+x}S_{16}$ (x=0~1.0) compounds with an excess of Sn, and examined their thermoelectric (TE) properties. The first principle calculation reveals that the excess Sn, which exhibits Sn^{2+} preferential to the intrinsic Cu vacancies, unpins the Fermi level (F_r) and allows the F_r to enter the conduction band (CB) at x=0.5. Accordingly, the Hall carrier concentration (n_H) has been enhanced by about two orders of magnitude with x value increasing from x=0 to x=0.5. Meanwhile, the lattice thermal conductivity (κ_L) has been reduced significantly to 0.39 $WK^{-1}m^{-1}$ at 893 K, which is in a good agreement with the estimation using Callaway model. As a consequence, the dimensionless TE figure of merit (ZT) of the compound $Cu_4Sn_{7+x}S_{16}$ with x=0.5 reaches 0.41 at 863 K. This value doubles that of the stoichiometric $Cu_4Sn_7S_{16}$, proving that the excess Sn in $Cu_4Sn_7S_{16}$ is beneficial to improve the TE performance.

Keywords: Band structure; Thermoelectric performance; Lattice thermal conductivity; $Cu_4Sn_7S_{16}$; Hall carrier concentration

INTRODUCTION

The conversion efficiency between heat and electricity is directly related to the material performance, mainly, the thermoelectric (TE) figure of merit (ZT), which is defined by

$$ZT=T\alpha^2\sigma / \kappa \qquad (1)$$

where T, α, σ and κ are the absolute temperature, Seebeck coefficient, electrical conductivity and total thermal conductivity respectively. In order to enhance the ZT value, we should increase the power factor $\alpha^2\sigma$ and simultaneously reduce the κ value which consists of electronic (κ_e) and lattice part (κ_L). Because the parameters α, σ, κ_e are interrelated, and are strongly dependent on the band structure, while the κ_L depends solely on the microstructures, it therefore is essential to engineer both the band structure[1-4] and the microstructures at the same time.[5,6]

Ternary copper tin chalcogenides form a large family of compounds, among which $Cu_4Sn_7S_{16}$ is one of the typical Cu-Sn-S ternary compounds reported with space group R-3m.[7-9] Because of its less expensive and earth abundant of three elements, along with the large Seebeck coefficient (~600 μVK^{-1} at room temperature)[8] and low thermal conductivity (~1.1 $Wm^{-1}K^{-1}$) [8], it has attracted much attention in the TE community in recent years. However, the experimentally determined highest ZT value is only 0.2 at 600 K.[8] This value is much low compared to those of the state-of-the-art TE materials, like SnSe, Bi_2Te_3- or PbTe-based alloys[10-13]. Therefore, there is a big room for improvement.

In the unit cell of $Cu_4Sn_7S_{16}$ (denominated by CTS), it has been reported that 3/4 of the tetrahedral sites and 1/8 of the octahedral sites are occupied by Cu^+, and 7/8 of the octahedral sites are occupied by Sn^{4+} ions.[7] This indicates that there are 1/4 of tetrahedral Cu vacancies unoccupied. Therefore, this compound can be formulated as $(Cu_{0.75}\square_{0.25})(Sn_{1.75}Cu_{0.25})S_4$, here □ represents vacancy.[7-9] Because the determined oxidation states of Cu, Sn and S in CTS are +1, +4 and -2, respectively,[7,9] the stoichiometric $(Cu^+)_4(Sn^{4+})_7(S^{2-})_{16}$ leads to total charge of zero. If the 1/4 of unoccupied Cu sites are incorporated by

* Corresponding authors:
cuijl@nbut.edu.cn, Tel: 86-0574-87080504, Fax: 86-0574-87080504

cationic elements, not only can the acceptor-like defect (Cu vacancies) be annihilated, but also does the Fermi level (*F*r) unpin.[14,15] Owing to the unpinning of the Fermi level, *F*r moves from the valence band maximum (VBM)[14] towards the conduction band minimum (CBM), which tunes the carrier concentration and improves the TE performance.[16] Moreover, the occupation of cationic elements would create multiple point defects and reduce the mean free path of phonons, leading to reduced lattice thermal conductivity (κ_L).

In this work, we have investigated the modifications of band structures using first principle calculation through the occupation of excess Sn or Cu in the unoccupied Cu sites in $Cu_4Sn_7S_{16}$, and then designed the composition of the materials in the experiments. Assuming the occupation of excess Sn in the Cu vacancies, we have observed that the semiconductor $Cu_4Sn_7S_{16}$ becomes a metallic-like material. Based on the calculation, we have observed that the *F*r moves the conduction band for a proper Cu content, which significantly enhances the carrier concentration and reduces the lattice contribution κ_L. The ZT value (0.41 at 863 K) therefore doubles that of stoichiometric $Cu_4Sn_7S_{16}$ (0.20 at 853 K) .

EXPERIMENTAL SECTION

Sample preparation Considering the thermal stability range (773-953 K)[17] of the compound $Cu_4Sn_7S_{16}$ and its less chemical potential stability range based on the calculated chemical potential phase space,[14,18] the synthetic route of $Cu_4Sn_7S_{16}$ needs a special modification, which is described below in detail. The mixtures of three elements Cu, Sn and S, according to the formula $Cu_4Sn_{7+x}S_{16}$ (x=0, 0.1, 0.2, 0.5 and 1.0), were loaded into five different vacuum silica tubes, and heated to 723 K in 4.5 h, followed by 2 h holding at this temperature. The tubes were slowly heated to reach temperature 1123 K in 4 h, and then kept at 1123 K for 4 h. Subsequently, the molten mixtures were cooled from 1123 K to 923 K in 1.5 h, and then held at 923 K for 24 h for the synthesis of the solid solution. Finally, the ingots at 923 K were cooled to room temperature (RT) in 7 h. With the above preparation procedure, the titled single phase materials can be formed. After ball milling of the ingots, the dried powders were quickly sintered by using spark plasma sintering apparatus (SPS−1030) with a designed sintering program under a pressure of 60 MPa. The densities of the sintered samples were measured by using Archimedes' method. Each sample was cut into 3−mm slices measuring 2.5 mm ×12 mm out of the sintered block with a size of ϕ 20 mm × 2.5 mm for electrical property measurements. After polishing the surfaces of two sides, the coin-shaped blocks with the size of ϕ 10 mm × 1.5 mm were prepared for thermal diffusivity measurements.

Physical property Measurements The physical properties including the Seebeck coefficients (α) and electrical conductivities (σ) were measured by using a ULVAC ZEM−3 instrument system under helium atmosphere from RT to ~900 K, with measurement uncertainties of ~6.0% on both the absolute values of the Seebeck coefficient and electrical conductivity. A temperature difference of around 5ºC has been applied to two terminals of the sample to measure the Seebeck coefficient, whereas the electrical conductivity was measured by using a four−probe method. The thermal diffusivities (λ) were measured by using TC−1200RH apparatus, with the uncertainties around 10%, and the heat capacities (C_p) were estimated using Dulong–Petit rule. The total thermal conductivities (κ) were calculated as the products of material densities (d), specific heats and thermal diffusivities.

$$\kappa = \ldots\ldots\ldots\ldots\ldots\ldots\ldots\ldots (2)$$

The three physical parameters (α,σ,κ) were finalized by taking the average values of several samples tested by the same method. The total uncertainty of the ZT value is about 18%. The lattice contributions (κ_L) were obtained by subtracting the electronic contribution (κ_e) from the total κ, i.e., $\kappa_L=\kappa-\kappa_e$. Here κ_e is expressed by

the Wiedemann–Franz law, $\kappa_e = L_0\sigma T$, where L_0 is the Lorenz number, estimated at $1.5\times10^{-8}W\Omega K^{-2}$ for not fully degenerate environment of semiconductors.[19] The Hall coefficient (R_H) measurements at RT were conducted on a Hall effect measurement system (PPMS, Model–9) by using a four–probe configuration with a magnetic field sweeping between ±5.0 T and then performed on rectangular samples with the size of $2\times2\times7$ mm^3. The Hall mobility (μ) and carrier concentration (n_H) were subsequently calculated according to the relationships $\mu = |R_H|\sigma$ and $n_H = -1/(e\,R_H)$ respectively, where e is the electron charge.

Chemical compositions and structural analyses The chemical compositions were determined using an electron probe micro-analyzer (EPMA) (S-4800, Hitachi, Japan) with an accuracy >97%.

The phases in the samples were analyzed by X-ray powder diffractometer (XRD) (D8 Advance) operating at 50 kV and 40 mA. Cu Kα radiation (λ=0.15406 nm) and a scan rate of 4° min^{-1} were used to record the patterns in the range of 10° to 100°.

X–ray photoelectron spectra (XPS) were measured on a AXIS ULTRA DLD equipped with a monochromatic Al Kα x–ray source (30 mA, 15 kV) and a hybrid lens. Samples were sputter–cleaned with an Ar^+ ion beam until core–level peaks associated with surface oxides were no longer observed in the XPS spectra. High–resolution core–level spectra Cu2*p*, Sn3*d*, and S2*p* on the sample $Cu_4Sn_{7.5}S_{16}$ were collected. $Cu_4Sn_7S_{16}$ (CTS) was also examined for comparison.

Raman spectra of three powdered $Cu_4Sn_{7+x}S_{16}$ samples (x=0, 0.2, 0.5) were recorded at 300 K from 50 to 4000 cm^{-1} at 0.6 cm^{-1} resolution using an Invia-Reflex Raman spectrometer with Nd:YAG laser source (l= 532.0 nm). A 50 × objective lens was employed via a confocal geometry to transmit the incident laser beam and collect the scattered radiation. Laser intensity was mandatorily attenuated to prevent the samples from decomposing.

The absorption coefficient (A) measurements were carried out using a Perkin–Elmer Lambda 950 UV-VIS-NIR spectrophotometer, and absorption spectra for the powders were recorded between the visible and infrared regions (200–1500 nm).[20]

First principle calculation Calculations were carried out using spin-polarized density functional theory (DFT) with generalized approximation (GGA) of Perdew–Burke–Ernzerhof (PBE)[21] implemented in the Vienna *ab* initio simulation package (VASP, version 5.2.12). [22,23] The DFT+U methodology with a value of U=5.0 eV was used in this work,[24] which has been utilized for $Cu_4Sn_7S_{16}$ in the literature. The valence electronic states were expanded in the basis of plane waves, with the core–valence interaction represented using the scalar relativistic projector augmented wave (PAW)[25] approach and a cutoff of 400 eV. A more accurate single point electronic structure calculation was further performed using the HSE06 function to obtain the density of states of the $Cu_{4+x}Sn_7S_{16}$ system.

RESULTS AND DISCUSSION

XRD and composition analyses

The x-ray diffraction (XRD) patterns of the titled powders are shown in Fig.S1, where the observed peak positions from $Cu_4Sn_{7+x}S_{16}$ powders ($x\leq0.5$) are the same as those from stoichiometric $Cu_4Sn_7S_{16}$ (PDF: 51-0932), indicating that the synthesized samples are crystallized in a single phase with the rhombohedral structure (*R*-3m). At x=1.0, an impurity phase Sn_3S_4 (PDF: 27-0900) has been identified, indicating that the solubility of Sn in CTS is less than 0.5 in the present materials. The calculated lattice parameters a (7.32~7.36 Å) and c (35.86~35.97 Å), which are in agreement with those reported,[8] increase linearly with Sn content increasing and follow the

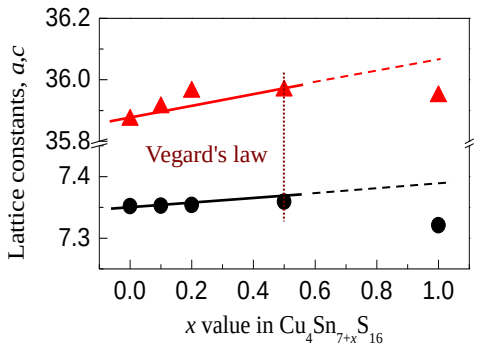

Figure 1. Lattice constants a and c as a function of excess Sn content (x value).

Vegard's law at $x \leq 0.5$ (see Fig.1), suggesting that the crystal lattice suffers dilation with excess incorporation of Sn. However, Vegard's law does not capture the *a* and *c* values at $x=1.0$, because the values at $x=1.0$ are much smaller than those at $x=0.5$. The decreasing of the *a* and *c* values at $x=1.0$ might be due to the formation of the impurity phase Sn_3S_4 shrinking the crystal lattice.

The chemical compositions for stoichiometric CTS and Sn-incorporated $Cu_4Sn_{7+x}S_{16}$ ($x=0.5$) taken from mappings of EPMA are shown in Table S1, where the number of S moles is normalized to 16. The mapping pictures of three elements are presented in Fig.S2(a-c). The line scan of $Cu_4Sn_{7.5}S_{16}$ ($x=0.5$) is shown in Fig.S2d. In Table S1 the relative molars of Cu, Sn, S identified are close to those of as-prepared materials, except for a little excess in Sn. In addition, the line scan analysis has revealed an almost homogeneous distribution of three elements in the $Cu_4Sn_{7.5}S_{16}$ matrix.

First principle calculation

In order to identify the site preference of excess Sn or Cu in the lattice, we have calculated the formation energies (E_f) and density of states (DOS) with an excess of Sn ($Cu_4Sn_{7+x}S_{16}$, $x=0$, 0.5, 1.0) and Cu ($Cu_{4+y}Sn_7S_{16}$, $y=0$, 0.5, 1.0) in CTS. In this work, we have calculated E_f values and DOS for the two different crystal structures (hexagonal and rhombohedral), and found the corresponding E_f values and DOS are almost identical. Therefore, we just present the results from the hexagonal crystal structure (shown in Fig.2a), while the rhombohedral structures are shown in Fig.S3. The left panel in Fig.2a is the unit cells of CTS with an excess of Sn, and right panel is that of CTS with an excess of Cu. The middle panel in Fig.2(a) represents the Cu vacancies in stoichiometric $Cu_4Sn_7S_{16}$ circled by blue lines. In the unit cell of CTS, there are total six Cu vacancies (1, 2 and 3), among which the tetrahedral sites are represented. Each Cu vacancy in the circle 1 is shared by four unit cells. Thus, only one vacancy in the circle 1 can be counted. The other two vacancies are circled by 2 and 3 respectively. Therefore, there are total 3 Cu vacancies in the unit cell. For the stoichiometric CTS, the Fermi level (*F*r) is just located in the valence band maximum (VBM), as shown in the middle of Fig.2b, which is in accordance with the calculations by Jemetio[9] and Zawadzki.[14] If Sn is in excess, the Fermi level (*F*r) enters conduction band (CB) with the bandgap (E_g) of ~0.55 eV ($x=0.5$). With Sn content increasing to $x=1.0$, deep impurity levels are observed near the middle of the bandgap (an inset is the close-up view of the impurity levels labeled by blue lines), see the left two panels in Fig.2b. Although such impurity levels seem to allow the reduction of the bandgap (E_g), they act as annihilation centers for electrons and holes, and thereby make no contribution to the carrier concentration. However, the bandgap is reduced to zero as Cu is in excess, as shown in the right two panels in Fig.2b, which exhibits a metallic behavior. Fig.2c is the corresponding total formation energy profile with excess of Sn or Cu in CTS, where the formation energy (E_f) drops remarkably in both samples with Sn or Cu in excess (E_f= -3.63 eV and -2.72 eV), suggesting that the excess Sn or Cu is energetically favorable to the Cu vacancies.

Upon proper Sn incorporation in the Cu vacancies, the Fermi level (*F*r) unpins, and is shifted to the conduction band, which suggests that the incorporated Sn acts as a donor, and responsible for the enhancement in carrier concentration.

In addition, the electronic charges of the Sn ions in the Cu vacancies are determined to be +2.2 *e* through Bader charge analysis, which suggests that the possible Sn ions in the Cu vacancies is the bivalent Sn.

XPS

Since the element Sn could exhibit mixed valence states in some compounds, such as the case in In_6Se_7,[16,26] it therefore is necessary to determine its oxidation states of the compound with an excess of Sn. Here we analyze the valence states of three elements using Cu$2p_{3/2}$, Sn$3d_{5/2}$, and S$2p_{3/2}$ XPS spectra, and the results are shown in Fig.S4 in the Supporting Information. The average binding energy (BE) values with uncertainties estimated at ~ ±0.01 eV are listed in Table S2, in which the BE values of Cu2p are ~932.30 eV

and 952.22 eV, with a peak separation of ~19.90 eV, indicating the presence of Cu^{+}.[27-29] The two peaks of the S2p XPS spectra in CTS or base material are ~161.55 eV and ~162.75 eV, with a peak separation of 1.20 eV, which are consistent with the expected values (160−164 eV) of S in sulfide phases. Hence, S^{2-} can be identified.[27-29] The BE values of $Sn3d_{5/2}$ and $Sn3d_{3/2}$ are around 486.35–486.50 eV and 494.60-494.85 eV, close to those of Sn^{2+} (486.30–486.60 eV for $Sn3d_{5/2}$)[30-34] and Sn^{4+} (494.35~494.50 eV for $Sn3d_{3/2}$),[34] indicate the presence of mixed valence states of Sn (Sn^{2+} and Sn^{4+}).

Combined with the Bader charge analysis, it is confirmed that the bivalent Sn is incorporated into the Cu vacancies.

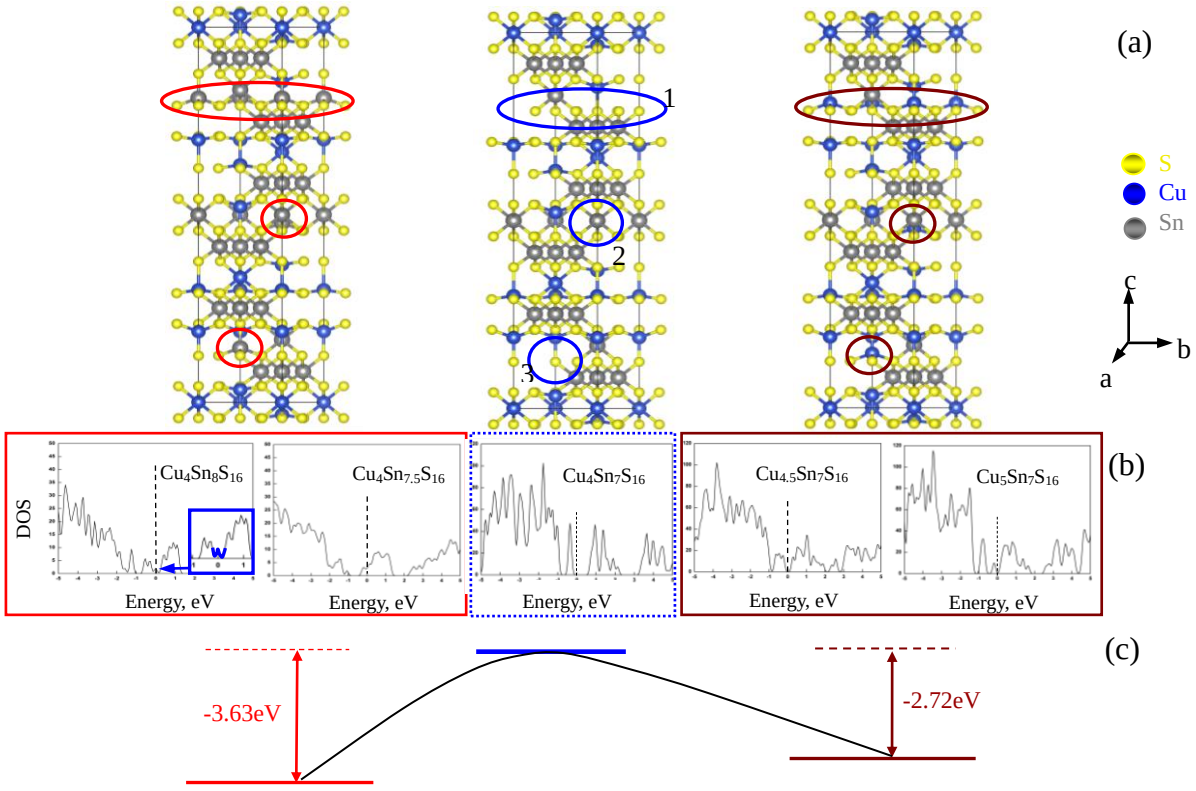

Figure 2. The results from the first principle calculation. (a) Hexagonal crystal structures upon the occupation of excess Sn ($Cu_4Sn_{7.5}S_{16}$, $Cu_4Sn_8S_{16}$) (left panel) or Cu (right panel) ($Cu_{4.5}Sn_7S_{16}$, $Cu_5Sn_7S_{16}$) in the vacancies in $Cu_4Sn_7S_{16}$. The enclosed by blue circles in the middle panel represent the Cu vacancies in stoichiometric $Cu_4Sn_7S_{16}$; (b) Density of States (DOS) for excess Sn (left two panels) or Cu incorporated $Cu_4Sn_7S_{16}$ (right two panels), indicating that the Fermi level (F_r) enters the conduction band for $Cu_4Sn_{7.5}S_{16}$, and deep impurity levels creates near the middle of the bandgap at $Cu_4Sn_8S_{16}$ (an inset is the close-up view of the impurity levels labeled by blue lines); With Cu content increasing, the bandgap gets narrower (right two panels), thereby a metallic behavior has been observed. (c) Overall total-formation energy (E_f) profile when the corresponding excess Sn or Cu is incorporated.

Raman spectra

In order to gain a deep insight of the cationic incorporation into the Cu vacancies, we have analyzed the Raman spectra of three samples (x=0, 0.2 and 0.5), which are shown in Fig.3, with the Raman spectrum of stoichiometric CTS for comparison. In the Raman spectra the modes at 181.7 cm^{-1}, 192 cm^{-1}, 274 cm^{-1}, 305 cm^{-1}, 311 cm^{-1}, 350 cm^{-1}, 365 cm^{-1} and 466 cm^{-1} appear for all configurations and remain active. It is worth noting that a red shift for the modes at 181.7 cm^{-1}, 192 cm^{-1}, 274 cm^{-1}, 305 cm^{-1}, 311 cm^{-1} has been observed,

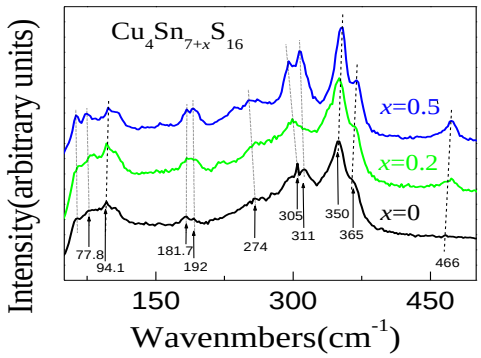

Figure 3. Raman spectra of $Cu_4Sn_{7+x}S_{16}$ (x =0, 0.2, 0.5) samples, a blue shift for the modes at 350 cm^{-1}, 365 cm^{-1} and 466 cm^{-1} has been observed with Sn content increasing; while the other modes 181.7 cm^{-1}, 192 cm^{-1}, 274 cm^{-1}, 305 cm^{-1}, 311 cm^{-1} show a red shift.

while a blue shift exists for the modes at 350 cm^{-1}, 365 cm^{-1} and 466 cm^{-1} with Sn content increasing. Since the Raman shift is related to the internal strain/stress within the compound and the compressive or tensile stress corresponds to blue or red shift respectively, the observed blue shift in the Raman peak at 350 cm^{-1}, 365 cm^{-1} and 466 cm^{-1} indicates the presence of compressive stress, while the red shift at 181.7 cm^{-1}, 192 cm^{-1}, 274 cm^{-1}, 305 cm^{-1}, 311 cm^{-1} suggests that excess Sn prefers the Cu vacancies leading to tensile stress. It is the Sn^{2+} occupying at Cu vacancies that creates the tensile stress and gives rise to the red shift.

Thermoelectric performance

To have a better understanding the role of the Sn^{2+}, we have measured the Hall coefficients (R_H) at RT. The measured R_H values are negative, indicating that the majority carriers are electrons. The calculated Hall carrier concentration (n_H) and mobility (μ) are shown in Fig.4a. With the Sn content increasing, the n_H value increases from 6.69 × 10^{14} cm^{-3} (x=0) to 4.48 × 10^{16} cm^{-3} (x=0.5), increasing by about two orders of magnitude, while the mobility μ value drops dramatically from 51.04 $cm^2V^{-1}s^{-1}$ (x=0) to 4.03 $cm^2V^{-1}s^{-1}$ (x=0.1), then saturated at x=0.2~0.5.

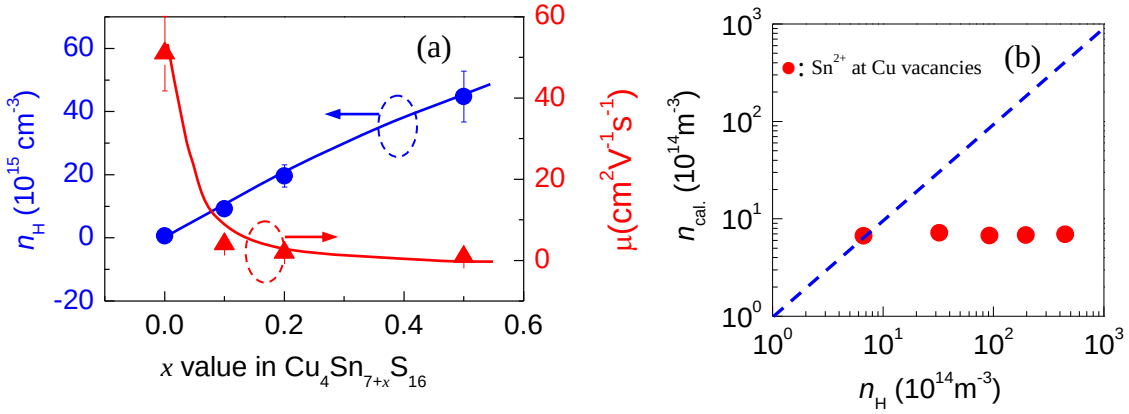

Figure 4. (a) Measured Hall carrier concentration (n_H) and mobility (μ) against x value in $Cu_4Sn_{7+x}S_{16}$. (b) Calculated theoretical carrier densities ($n_{cal.}$) upon Sn^{2+} occupation in the Cu vacancies against Hall carrier concentration (n_H).

The enhancement in n_H value with Sn content increasing (x≤0.5) might be attributed to the alteration of chemical environment upon preferential occupation of Sn in the Cu vacancies. If this is the case, we believe that the extra positive charge introduced by Sn^{2+} should be equal to x/14, according to the formula below,

$(Cu^+)_4\boxed{Sn^{2+}_x}(Sn^{4+})_7(S^{2-})_{16}$ (x≤0.5) (3)

Therefore, the theoretical carrier density n_{cal} can be calculated as, $n_{cal} = n_{CTS}(1+x/14)$, where n_{CTS} is the Hall carrier concentration of CTS. The results are shown in Fig.4b. However, there is no agreement between the measured Hall carrier concentrations n_H and the calculated n_{cal} values. The measured n_H values at RT are about 1~2 orders of magnitude higher than the calculated n_{cal}, which indicates that the enhanced carrier

density in the present materials is not resulted from the alteration of chemical environment.

Fig.5(a) displays the Seebeck coefficients (α) against the temperature. The α values are negative, indicating the n-type semiconductor behavior of the materials. The absolute $|\alpha|$ value decreases with temperature increasing. At $T \geq 750$ K the sample with high Sn content gives relatively high $|\alpha|$ values. At 893 K the sample at x=0.5 gives the $|\alpha|$ value 334.1 ($\mu V\ K^{-1}$). The electrical conductivity (σ) bears a resemblance to the $|\alpha|$ value because the σ value increases with Sn content increasing. At 893 K the σ value is $1.56 \times 10^3 \Omega^{-1}m^{-1}$ for the sample at x=0.5.

Upon excess Sn incorporation into the Cu vacancies, the lattice part κ_L decreases almost linearly with temperature increasing, indicating that the phonon scattering mechanism is dominated by the Umklapp process. Besides, the κ_L value reduces with Sn content increasing. The more the Sn content is incorporated, the lower the κ_L value is at entire temperature range. The κ_L value for the sample at x=0.5 is reduced from 0.51 ($WK^{-1}m^{-1}$) at RT to 0.39 ($WK^{-1}m^{-1}$) at 893 K, while that for the sample at x=0 decreases from 0.62 ($WK^{-1}m^{-1}$) at RT to 0.47 ($WK^{-1}m^{-1}$) at 883 K (Fig.5c). The inset in Fig.5(c) is the total thermal conductivity κ as a function of temperature, which presents the almost identical dependence to κ_L, suggesting that the heat transport is dominated by phonons in the materials.

Combined with the three physical parameters (α, σ, κ) measured, we have attained the dimensionless figure of merit (ZT) for different samples, which are shown in Fig.5(d). Owing to the highest α, σ values and low κ values at x=0.5, the highest ZT value of 0.41 is obtained at 863 K. This is a doubled value of the stoichiometric CTS sample at 853 K and that of the reported value in literature [8]. This ZT value also stands the highest among known $Cu_4Sn_7S_{16}$ based alloys, suggesting that the excess Sn in $Cu_4Sn_7S_{16}$ plays a significant role in improving the TE performance.

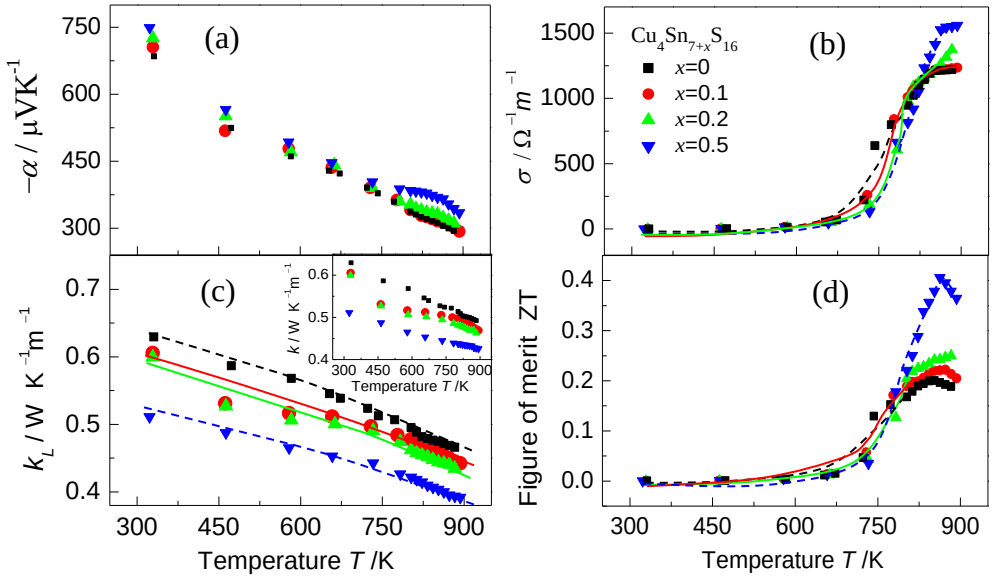

Figure 5. TE properties as a function of temperature, (a) Seebeck coefficient (α); (b) Electrical conductivity (σ); (c) lattice thermal conductivity (κ_L), the inset is the total κ; (d) ZT values.

In Fig.4a and Fig.5a, we have observed that both the n_H and $|\alpha|$ value have been enhanced with Sn content increasing. This implies that the single parabolic band model (SPB) breaks down, and fails to describe the relationship between the carrier concentration and Seebeck coefficient. Although the site preference of excess Sn results in a limited change in bandagp (E_g), with the measured E_g values of around 1.0~1.2 eV, almost independent on the Sn content ($x \leq 0.5$), see Fig.S5 and Fig.2, we have observed that the

Fermi level (*Fr*) has shifted into the conduction band with Sn content increasing to x=0.5. Therefore, it is believed that the Fermi level unpins solely upon cationic Sn incorporation without any tailing in the valence band. That is the reason why we have observed the enhancement of the carrier concentration with Sn content increasing ($x \leq 0.5$). The decreasing of the mobility (μ) might be due to the increased scattering of carriers in point defects[35,36] and local strain or stress[37] created nearby Cu vacancies.

The increased point defects and local strain (stress) give a profound impact on the lattice thermal conductivity (κ_L) as well, as the κ_L value generally decreases with Sn content increasing over the entire temperature range. In order to have a better understanding on the composition dependent of κ_L values, we estimate the variation tendency of the κ_L value based on the model proposed by Callaway et al.,[38] that is,

$$\kappa_L = \frac{K}{2\pi^2 v_s (ACT)^{\frac{1}{2}}} Tan^{-1}\left[\frac{K\theta}{\hbar}\left(\frac{A}{CT}\right)^{\frac{1}{2}}\right] \quad (4)$$

where A is a composition related parameter, and is defined by:

$$A = \frac{\Omega}{4\pi v_s^3} c(1-c)\left(\frac{\Delta M}{M}\right)^2 \quad (5)$$

K is the Boltzmann's constant, C is a constant, v_s is the velocity of sound (3.65×10^3 m/s),[8] which is not varying with composition., Ω is the volume of the unit cell, θ is the Debye temperature (395 K)[8] and c is the relative concentration of pure material ($0.5<c<1.0$ in the present solid solutions). Some parameters for different x value in compounds $Cu_4Sn_{7+x}S_{16}$ are shown in Table 1. The estimated κ_L values (labeled by dotted lines) as a function of x at near RT, 580 K and 893 K using Callaway model are shown in Fig.6, in which the estimated κ_L values are in good agreement with the experimental data, except that the κ_L values at low x values ($x \leq 0.1$). This confirms that the Callaway model works well in the present material system, assuming that the existing phonon scattering mechanism consists of the Umklapp scattering and point defect scattering mainly, if the following factors are taken into considerations: the binding force difference and strain field induced by the point defect in the present solid solutions.[38-41]

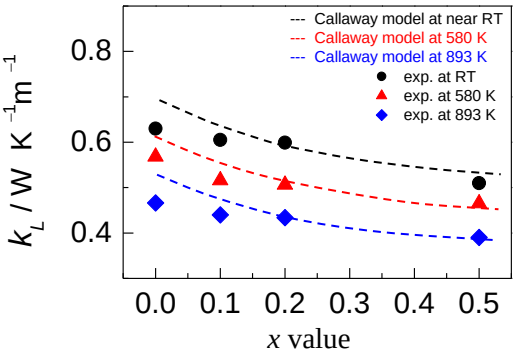

Figure 6 The lattice contributions (κ_L) labeled by ●,▲,♦ represent the present materials at RT, 580 K and 893 K, respectively, as a function of x value. The dotted lines represent the κ_L values at RT, 580 K and 893 K, estimated using Callaway et al.[38] model in solid solutions.

Table 1 Some parameters of different compounds $Cu_4Sn_{7+x}S_{16}$

	Ω, $10^{-27}m^3$	c	ΔM / M	$c(1-c)\Omega(\Delta M/M)^2$, $10^{-33}(m^3)$
x=0	1.9388	1.0	-------	-------
x=0.1	1.9413	0.9938	0.0129	2.0292
x=0.2	1.9448	0.9988	0.0259	1.6345
x=0.5	1.9477	0.9688	0.0648	248.10

CONCLUSION

In this work we have synthesized ternary $Cu_4Sn_7S_{16}$ compounds with different Sn and Cu in excess, and examined the band structures and TE performance of $Cu_4Sn_{7+x}S_{16}$. The first principle calculation reveals that the excess Sn has a site preference in the Cu vacancies with the oxidation state Sn^{2+} acting as donors. The occupation of Sn^{2+} unpins the Fermi level (F_r), and allows the F_r entering into the conduction band. Therefore, the carrier concentration n_H has been enhanced by about two orders of magnitude with Sn content increasing from x=0 to x=0.5. The lattice contribution κ_L has been reduced with Sn content increasing, and is in a good agreement with the estimation using Callaway model for solid solutions. As a consequence, the thermoelectric figure of merit (ZT) of the compound $Cu_4Sn_{7+x}S_{16}$ (x=0.5) (ZT=0.41 at 863 K) has a doubled value of stoichiometric $Cu_4Sn_7S_{16}$ (ZT=0.20 at 853 K).

AUTHOR INFORMATION

Corresponding Authors

*Jiaolin Cui. Address: School of Materials & Chemical Engineering, Ningbo University of Technology, Ningbo, 315016, China. E-mail: cuijiaolin@163.com.

*Naiming Lin. Address: Materials Science and Engineering College, Taiyuan University of Technology, Taiyuan, 030024, China. E-mail: linnaiming@tyut.edu.cn.

*Yimin Chao. Address: School of Chemistry, University of East Anglia, Norwich NR4 7TJ, United Kingdom. E-mail: Y.Chao@uea.ac.uk.

Author Contributions

Tongtong He and Naiming Lin prepared materials & samples and performed experiments on thermoelectric properties; Zhengliang Du analyzed chemical compositions, XRD patterns, XPS and Raman spectra etc.; Jiaolin Cui was in charge of designing the study and whole experimental work, and Yimin Chao helped to design the study and revise the manuscript.

Notes

The authors declare no competing financial interest.

ACKNOWLEDGMENTS

This work is supported by the National Natural Science Foundation of China (51671109, 51171084), Zhejiang Provincial Natural Science Foundation (LY14E010003, LQ14E010001), and Natural Science Foundation of Ningbo (2015A610044). We are also grateful for the first principles calculations from Dr. Z.K. Han (Shanghai Institute of Applied Physics, Chinese Academy of Sciences).

Supporting Information Available: including X-ray diffraction patterns of $Cu_4Sn_{7+x}S_{16}$ (x=0~1.0), EPMA mappings of three elements on polished $Cu_4Sn_{7.5}S_{16}$ surface, line scanning analysis of the chemical compositions, X-ray photoelectron spectroscopy spectra and Measured bandgap (E_g) determined by using the $(Ahv)^2$~(hv) relation. This material is available free of charge via the Internet at http://pubs.acs.org.

REFERENCES

(1) Pei, Y.; Shi, X.; LaLonde, A.; Wang, H.; Chen, L.; Snyder, G. J. Convergence of Electronic Bands for High Performance Bulk Thermoelectrics. *Nature* **2011**, *473*, 66-69.

(2) Liu, W.; Tan, X.; Yin, K.; Liu, H.; Tang, X.; Shi, J.; Zhang, Q.; Uher, C. Convergence of Conduction Bands as a Means of Enhancing Thermoelectric Performance of n-Type $Mg_2Si_{1-x}Sn_x$ Solid Solutions. *Phys. Rev. Lett.* **2012**, *108*, 166601.

(3) Lin,S.; Li,W.; Chen,Z.; Shen,J.; Ge,B.; Pei,Y. Tellurium as a High-performance Elemental Thermoelectric. *Nat. Commun*, **2016**, *7*, 10287.

(4) Pei, Y.; LaLonde, A. D.; Wang, H.; Snyder, G. J. Low Effective Mass Leading to High Thermoelectric Performance. *Energy Environ. Sci*, **2012**, *5*, 7963-7969.

(5) Tang, G.; Wei, W.; Zhang, J.; Li,Y.; Wang, X.; Xu, G.; Chang, C.; Wang, Z.; Du, Y.; Zhao, L. Realizing High Figure of Merit in Phase-Separated Polycrystalline $Sn_{1-x}Pb_xSe$. J. Am. Chem. Soc. **2016**, *138*, 13647−13654.

(6) Biswas,K.; He,J.Q.; Blum,I.D.; Chun,I.W.; Hogan,T.P.; Seidman,D.N.; Dravid,V.P.; Kanatzidis, M.G. High-Performance Bulk Thermoelectrics with All-Scale Hierarchical Architectures. *Nature 2012*, **490**, 414-418.

(7) Chen, X.; Wada,H.; Sato, A,; Mieno, M. Synthesis, Electrical Conductivity, and Crystal Structure of $Cu_4Sn_7S_{16}$ and Structure Refinement of Cu_2SnS_3. *J. Solid State Chem*. **1998**,*139*, 144-151.

(8) Bourgès, C,; Lemoine, P,; Lebedev,O. I.; Daou, R.; Hardy,V,; Malaman, B,; Guilmeau, E. Low Thermal Conductivity in Ternary $Cu_4Sn_7S_{16}$ Compound. *Acta Mater*. **2015**, *97*, 180–190.

(9) Jemetio, J. P. F.; Zhou, P.; Kleinke,H. Crystal Structure, Electronic Structure and Thermoelectric Properties of $Cu_4Sn_7S_{16}$. *J. Alloys Compds*. **2006**, *417*, 55–59.

(10) Zhao,L.; Tan,G.; Hao,S.; He,J.; Pei,Y.; Chi,H.; Wang,H.; Gong,S.; Xu,H.; Dravid,V.P.; Uher,C.; Snyder,G.J.; Wolverton,C.; Kanatzidis, M.G. Ultrahigh Power Factor and Thermoelectric Performance in Hole-doped Single-crystal SnSe. *Science* **2016**,*351*,141-144

(11) Zhao,L.; Lo,S.; Zhang,Y.; Sun,H.; Tan,G.; Uher,C.; Wolverton,C.; Dravid, V.P.; Kanatzidis,M.G. Ultralow Thermal Conductivity and High Thermoelectric Figure of Merit in SnSe crystals. *Nature* **2014**,*508*, 373-389.

(12) Poudel,B.; Hao,Q.; Ma,Y.; Lan,Y.; Minnich,A.; Yu,B.; Yan,X.; Wang,D.; Muto,A.; Vashaee,D.; Chen,X.; Liu,J.; Dresselhaus,M.S.; Chen,G.; Ren,Z. High-Thermoelectric Performance of Nanostructured Bismuth Antimony Telluride Bulk Alloys. *Science*, **2008**, *320*, 634-638.

(13) Hsu,K.F.; Loo,S.; Guo,F.; Chen,W.; Dyck,J.S.; Uher,C.; Hogan,T.; Polychroniadis,E.K.; Kanatzidis, M.G. Cubic $AgPb_mSbTe_{2-m}$: Bulk Thermoelectric Materials with High Figure of Merit. *Science* **2004**,*303*, 818–821.

(14) Zawadzki,P.; Baranowski, .L.; Peng,H.; Toberer,E.S.; Ginley, D.S.; Tumas,W.; Zakutayev,A.; Lany,S. Evaluation of Photovoltaic Materials Within the Cu-Sn-S Family. *Appl. Phys. Lett*. **2013**, *103*, 253902.

(15) Persson,C.; Zhao,Y.; Lany,S.; Zunger, A. *N*-type Doping of $CuInSe_2$ and $CuGaSe_2$. *Phys. Rev. B* **2005**, *72*, 35211.

(16) Cui,J,; Cheng,M,; Wu,W,; Du,Z,; Chao,Y. Engineering Band Structure via the Site Preference of Pb^{2+} in the In^+ Site for Enhanced Thermoelectric Performance of In_6Se_7. *ACS Appl. Mater. Interfaces* **2016**, *8*, 23175−23180.

(17) Fiechter,S.; Martinez,M.; Schmidt,G.; Henrion,W.; Tomm,Y. Phase Relations and Optical Properties of Semiconducting Ternary Sulfides in the System Cu–Sn–S, *J. Phys. Chem. Solids* **2003**, *64*, 1859–1862.

(18) Baranowski,L.L.; Zawadzki,P.; Christensen,S.; Nordlund,D.; Lany,S.; Tamboli,A.C.; Gedvilas,L.; Ginley,D.S.; Tumas,W.; Toberer,E.S.; Zakutayev,A. Control of Doping in Cu_2SnS_3 through Defects and Alloying. *Chem. Mater*. **2014**, *26*, 4951−4959.

(19) Shi, X.; Chen, L.; Uher, C. Recent Advances in High-performance Bulk Thermoelectric Materials. *Inter. Mater. Rev*. **2016**, *61*, 379–415.

(20) Colakoğlu,T.; Parlak,M. Structural Characterization of Polycrystalline Ag–In–Se Thin Films Deposited by E-beam Technique. *Appl. Surf. Sci*. **2008**, *254*, 1569-1577.

(21) Perdew,J.; Burke,P. K.; Ernzerhof,M. Generalized Gradient Approximation Made Simple. *Phys. Rev. Lett*. **1996**, *77*, 3865-3868.

(22) Kresse,G.; Furthmuller,J. Efficient Iterative Schemes for *ab initio* Total-energy Calculations Using a Plane-wave Basis Set. *Phys. Rev*. *B* **1996**, *54*, 11169 –11186.

(23) Kresse,G.; Furthmuller,J. Efficiency of ab-initio Total Energy Calculations for Metals and Semiconductors Using a Plane-wave Basis Set. *Comput. Mater. Sci*. **1996**, *6*, 15–50.

(24) Nolan,M.; Parker,S. C.; Watson,G.W. The Electronic Structure of Oxygen Vacancy Defects at the Low Index Surface of Ceria. *Surf. Sci*. **2005**, *595*, 223 –232.

(25) Blöchl,P.E. Projector Augmented-wave Method. *Phys. Rev. B*: *Condens. Matter* **1994**, *50*, 17953-17979.

(26) Cheng, M.; Chen,S.; Du,Z.; Liu,X.; Cui, J. Improvement in Thermoelectric Performance of In_6Se_7 by Substitution of Sn for In. *Phys. Status Solidi A* **2016**, *213*, 2176–2182.

(27) Xu, J.; Yang,X.; Yang,Q.; Wong,T.; Lee,C. Cu_2ZnSnS_4 Hierarchical Microspheres as an Effective Counter Electrode Material for Quantum Dot Sensitized Solar Cells. *J. Phys. Chem. C* **2012**, *116*, 19718−19723.

(28) Riha, S.C.; Parkinson,B.A.; Prieto,A.L. Solution-Based Synthesis and Characterization of Cu_2ZnSnS_4 Nanocrystals. *J.Am.Chem.Soc*. **2009**, *131*, 12054–12055.

(29) Calderón,C.; Gordillo,G.; Becerra,R.; Bartolo-Pérez, P. XPS Analysis and Characterization of Thin Films Cu_2ZnSnS_4 Grown Using a Novel Solution Based Route. *Mater. Sci. Semicon. Proc*. **2015**, *39*, 492–498.

(30) J. F. Moulder and J. Chastain, Handbook of X-ray Photoelectron Spectroscopy: A Reference Book of Standard Spectra for Identification and Interpretation of XPS Data (Perkin-Elmer Corporation, Physical Electronics Division, Eden Prairie, Minnesota) **1992**, 92.

(31) Hosogi,Y.; Shimodaira,Y.; Kato,H.; Kobayashi,H.; Kudo,A. Role of Sn^{2+} in the Band Structure of SnM_2O_6 and $Sn_2M_2O_7$ (M = Nb and Ta) and Their Photocatalytic Properties. *Chem. Mater*. **2008**, *20*, 1299-1307.

(32) Maestre,D.; Cremades,A.; Gregoratti,L.; Piqueras,J. Indium Tin Oxide Micro- and Nanostructures Grown by Thermal Treatment of InN/SnO_2. *J. Phys. Chem. C* **2010**, *114*, 3411-3415.

(33) Naumkin,A.V.; Vass,A.K.; Gaarenstroom,S.W.; Powell,C.J. Distribution by the Measurement Service Divisions of the National Institute of Standards and Technology (NIST), Material Measurement Laboratory (MML), U.S. Department of Commerce, **2012**, 9.

(34) Themlin,J.; Chtaib, M.; Henrard,L.; Lambin,P.; Darville,J.; Gilles,J. Characterization of Tin Oxides by X-ray-photoemission Spectroscopy. *Phys. Rev. B* **1992**, *46*, 2460-2466.

(35)Yamini,S.A.; Wang,H.; Ginting,D.; Mitchell,D.R.G.; Dou,S.X.; Snyder,G.J. Thermoelectric Performance of n-Type $(PbTe)_{0.75}(PbS)_{0.15}(PbSe)_{0.1}$ Composites. *ACS Appl. Mater. Interfaces* **2014**, *6*, 11476−11483.

(36) Tan,G.; Shi,F.; Hao,S.; Chi,H.; Bailey,T.P.; Zhao,L.; Uher,C.; Wolverton,C.; Dravid,V.P.;

Kanatzidis,M.G. Valence Band Modification and High Thermoelectric Performance in SnTe Heavily Alloyed with MnTe. *J. Am. Chem. Soc*. **2015**, *137*, 11507−11516.

(37) He,J.; Girard,S.N.; Kanatzidis, M.G.; Dravid,V.P. Microstructure-Lattice Thermal Conductivity Correlation in Nanostructured $PbTe_{0.7}S_{0.3}$ Thermoelectric Materials. *Adv. Funct. Mater*. **2010**, *20*, 764–772.

(38) Callaway,J.; Baeyer, H.C.von Effect of Point Imperfections on Lattice Thermal Conductivity. *Phys. Rev*. **1960**, *120*, 1149-1154.

(39) Wang,H.; LaLonde, A.D.; Pei,Y.; Snyder,G. J. The criteria for Beneficial Disorder in Thermoelectric Solid Solutions. *Adv. Funct. Mater.* **2013**, *23*,1586-1596.

(40) R. Berman, *Thermal Conduction in Solids*, Oxford University Press , Oxford, **1976**.

(41) Toberer,E.S.; Zevalkink,A.; Snyder,G.J. Phonon Engineering through Crystal Chemistry. *J. Mater. Chem.* **2011**, *21*, 15843-15852.